A computational study of ion conductance in the KcsA K+ channel using a Nernst–Planck model with explicit resident ions

Yong-Woon Jung,[1,a)] Benzhuo Lu,[2] and Michael Mascagni[1,3]

[1]*Department of Mathematics, Florida State University, Tallahassee, Florida 32306-4510, USA*
[2]*Institute of Computational Mathematics and Scientific/Engineering Computing, Academy of Mathematics and Systems Science, Chinese Academy of Sciences, Beijing 100190, China*
[3]*Departments of Computer Science and Scientific Computing, Florida State University, Tallahassee, Florida 32306-4530, USA*

The biophysical mechanisms underlying the relationship between the structure and function of the KcsA K+ channel are described. Because of the conciseness of electrodiffusion theory and the computational advantages of a continuum approach, the Nernst–Planck (NP) type models, such as the Goldman–Hodgkin–Katz and Poisson-NP (PNP) models, have been used to describe currents in ion channels. However, the standard PNP (SPNP) model is known to be inapplicable to narrow ion channels because it cannot handle discrete ion properties. To overcome this weakness, the explicit resident ions NP (ERINP) model was formulated, which applies a local explicit model where the continuum model fails. Then, the effects of the ERI Coulomb potential, the ERI induced potential, and the ERI dielectric constant for ion conductance were tested in the ERINP model. The current-voltage (*I-V*) and current-concentration (*I-C*) relationships determined in the ERINP model provided biologically significant information that the traditional continuum model could not, explicitly taking into account the effects of resident ions inside the KcsA K+ channel. In addition, a mathematical analysis of the K+ ion dynamics established a tight structure-function system with a shallow well, a deep well, and two K+ ions resident in the selectivity filter. Furthermore, the ERINP model not only reproduced the experimental results with a realistic set of parameters, but it also reduced CPU costs. © *2009 American Institute of Physics*. [doi:10.1063/1.3268774]

I. INTRODUCTION

With the arrival of primitive lipid membranes, new transport mechanisms evolved to allow ionized substrates into the cell and release ionized waste products into the environment.[1] For the membrane to retain vital cell components, the transport device had to be small, but large enough for all small metabolites to cross it.[1] Subsequently, over billions of years of evolution,[1] these transport mechanisms evolved into highly sophisticated single file (the ion and water cannot get past each other) transport devices such that every living cell in nearly all organisms now has hundreds or even thousands of different kinds of ion channels.[2] Ion channels are major drug targets because they are involved in crucial physiological activities, such as heartbeat, breathing, and thinking, by adjusting the electrical charges inside and outside of cells. Based on their medical importance and recently discovered high-resolution structural information, many theoretical and computational studies using techniques such as molecular dynamics (MD) and Brown dynamics (BD) simulations or the Poisson–Nernst–Planck (PNP) model[3] have been conducted to elucidate the molecular mechanisms underlying ion conduction [K+ channels conduct ions at a rate approaching 10^8 ions s^{-1} (Ref. 4)] and selectivity (conduct their namesake ions while blocking others) at atomic level.

To understand the conductance mechanism, the KcsA (the K+ channel from *Streptomyces lividans*[5]) K+ channel was chosen as the physical system. Since 1998, the structure of the KcsA K+ channel has been extensively investigated in channel pharmacology research as a template for eukaryotic K+ channels. Also, the steady-state NP-type model was chosen over an ion channel model, not only because the model has the fascinating advantage of providing a concise electrodiffusion theory of ions traversing through a channel, but also because it can be computationally solved very efficiently. However, the current obtained from the PNP model in narrow ion channels has been known to be inaccurate.[6–11] There are three basic reasons: (1) the application of the standard PNP (SPNP) self-consistent approach to single file ion channels is problematic because the mean-field approximation relating the electric potential to the ion concentration breaks down; (2) in narrow cation channels, even a few resident cations significantly increase the positive electric potential because the continuum model unnecessarily redistributes spurious self-energy inside the channel[12] [see Fig. 6(a)]; and (3) the explicit resident ions (ERI) potentials (the ERI Coulomb and induced potentials) are disregarded because ions are treated as if they are at an average concentration. To overcome these weaknesses of the SPNP model, which does not handle discrete ion properties, a quasicontinuum (coupled atomistic and continuum) model was required. For this reason, the ERINP model was formulated (see Fig. 1).

A major component of this study was the proposal of

a)Author to whom correspondence should be addressed. Electronic mail: yjung@math.fsu.edu.
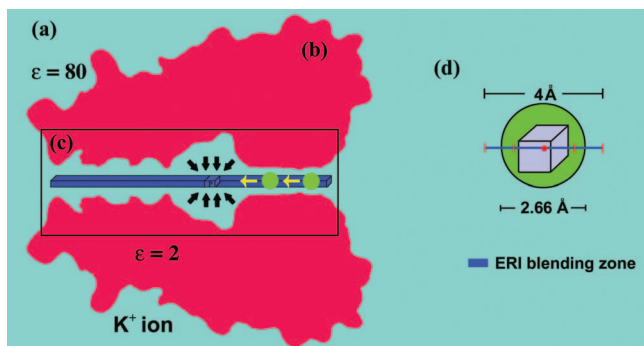
     131, 215101-1

FIG. 1. The formulation of the ERINP model. In general, the dielectric constants of the water and channel continua used to be set at 80 and 2 (Ref. 13), respectively, where the dielectric constant of vacuum is defined as 1. (a) Water continuum. (b) KcsA K$^+$ channel continuum [this closed channel was modeled as an open channel using the OPENDX software package (Ref. 14)]. Here, the potential arising from the membrane was ignored because it had no apparent charges and was distant from the channel pore. (c) The ERI potential zone. The black arrows denote the channel permanent potential assigned to 45 small ($1 \times 1 \times 1$ Å^3) cubic boxes (the length of the channel is 45 Å) lined up in the channel pore. The yellow arrows denote the ERI potentials of the two resident ions. (d) The ERI blending zone. A K$^+$ ion with a radius of 1.33 Å, which is in fact fluctuating, occupies three grid points.

plausible channel conductance mechanism by comparing two channel models [the Goldman–Hodgkin–Katz (GHK) model versus the ERINP model] and two ion states [the two-ion state (with two resident ions) versus the three-ion state (with three resident ions)]. A number of interesting questions were addressed in the ERINP model. In particular:

(1) How many K$^+$ ions reside in the channel and where do they prefer to reside? (see Fig. 5.)
(2) Are the ion positions with minimum energy related to high ionic throughput? (see Fig. 6.)
(3) How, and with what strategies, does the channel permanent potential increase the current? (see Fig. 7.)

The purposes of this paper are to: (1) present a quasicontinuum model (ERINP model) that is able to elucidate the nonequilibrium potential (arising during ion flow) inside single file ion channels; (2) investigate the intrinsic role of the channel permanent potential for overcoming the dielectric barrier presented by the cell membrane; and (3) establish a structure-function system based on the K$^+$ ion dynamics.

The layout of the paper is as follows. In Sec. II, the ERINP model and the GHK model[15] are introduced. In Sec. III, the physical system and the method for obtaining the channel permanent potential are illustrated. In addition, basic concepts of the ERI induced potential as well as the membrane potential and the ion concentration are described. In Sec. IV, using the ERI Coulomb potential, the scaled ERI induced potential, and the ERI dielectric constant, several ion conductance tests (two channel models and two ion states) are performed and their results are analyzed. In addition, a mathematical analysis of the K$^+$ ion dynamics is applied to relate the channel structure to its function. Finally, conclusions and discussions are briefly summarized in Sec. V.

II. THEORY AND METHODS

A. The NP-type model

Continuum NP-type models have fewer computational degrees of freedom compared to MD and BD techniques. In this NP-type model, the current depends on applied potential and concentration differences across the channel. The ion channel is so narrow that the motion in the x and y directions reaches equilibrium rapidly,[16] leaving the cations to navigate along the channel solely in the central z-axis (the reaction line).[17] Therefore, the flux in 3D, which is defined as J(x, y, z), is reduced to 1D $J(z)$.

To apply the 1D steady-state NP-type model, the structure of the channel pore was defined as a cylinder of varying cross-sectional area $[A(z)]$ along its z-axis, and I (the current) was assumed uniform across $A(z)$, which can be expressed as $I = eJ(z)A(z)$ [where e denotes the electron charge, $J(z)$ denotes the flux, and the monovalent cation valence is set at 1]. Thus, the NP equation[1] (or the current density equation), using two electrochemical gradients (when a self-consistent electric potential is applied to the NP equation, it becomes the PNP model), is expressed as

$$I = -eD\left(\frac{dn}{dz} + \frac{en}{kT}\frac{d\phi}{dz}\right)A(z), \tag{1}$$

where D denotes the diffusion coefficient assumed independent of z (obtained from the Einstein relation $D = kT/m\gamma$; k denotes the Boltzmann factor, T denotes the temperature, m denotes the ion mass, and γ denotes the friction coefficient)[18] and n and ϕ denote the ion concentration and the electric potential around the channel, respectively. Note that ϕ is the nonequilibrium potential arising when ions flow and is not constant because of thousands of charged atoms that comprise ion channels.

After $A(z)$ was put on the left hand side of Eq. (1), the modified equation was integrated from 0 to L (L is the length of an ion channel) using the integrating factor $e^{\Psi(z)}[\Psi(z) = (e/kT)\phi(z)]$. Thus, in a cylindrical channel of varying $A(z)$, the NP current equation has the following relationship:

$$I = -eD\frac{[n(L)e^{\Psi(L)} - n(0)e^{\Psi(0)}]}{\displaystyle\int_0^L \frac{e^{\Psi(z)}}{A(z)}dz}. \tag{2}$$

When the electric field is constant, Eq. (2) becomes the GHK current equation, which resulted in the following form:

$$I = -eD\frac{[n(L) - n(0)e^V]}{\displaystyle\int_0^L \frac{e^{V[(L-z)/L]}}{A(z)}dz}, \tag{3}$$

where $V_{\text{applied}} = \Psi(0) - \Psi(L)$.

Then, the remaining problem is to find 1D nonequilibrium potential $[\Psi(z)]$ of the central z-axis. To handle the discrete potential $[\Psi(z)]$ obtained from the Poisson solver, the numerical composite trapezoidal rule was applied to both Eqs. (2) and (3). The SPNP model using a self-consistent approach is well reviewed in recent PNP studies.[3,11,19,20]
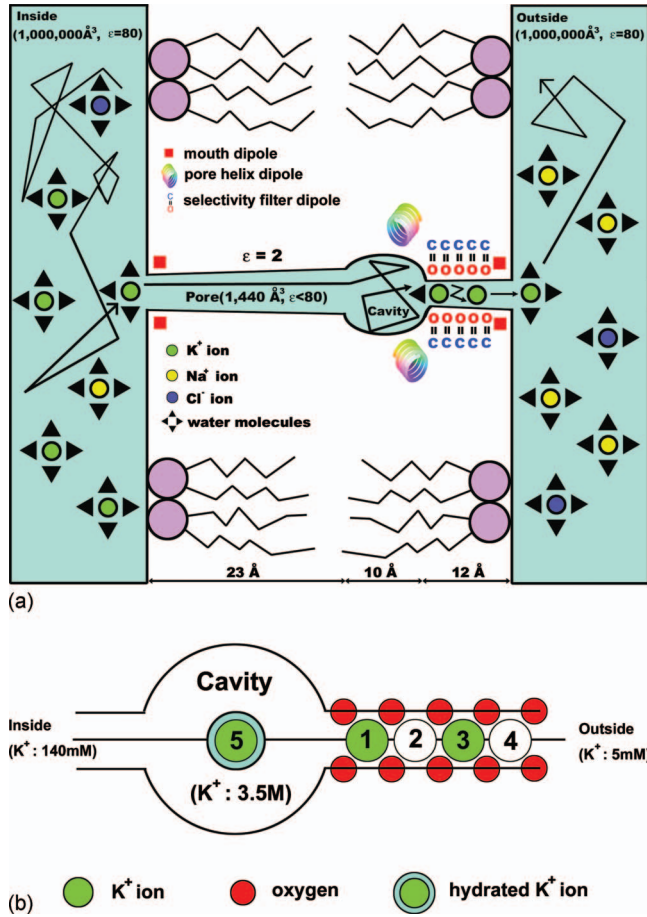
FIG. 2. (a) Electrohydrodynamic process in the KcsA K$^+$ channel. (b) A set of three K$^+$ ions in five binding sites.

B. Formulation of the ERINP model

Figure 1 presents the ERINP model, which applies a local explicit model where the continuum model fails. To find $\Psi(z)$ without using a self-consistent approach, the model treats a few resident K$^+$ in the selectivity filter (or filter) as particles and the rest of the system as continua. Because millions of ions cross this nanoscale channel every second, the current can be measured statistically (e.g., the diffusion coefficient is used for this purpose in the NP-type models). The first step is working out the average of all possible potentials arising from the position of each ion resident in the channel pore. According to the Boltzmann equation, as shown in Eq. (4), at equilibrium (or at quasiequilibrium), a particle spends more time in lower energy states than in higher energy states.

$$\frac{P_2}{P_1} = e^{-[(U_2 - U_1)/kT]}, \tag{4}$$

where P_2 and P_1 are the relative probabilities of finding a particle in state 2 and in state 1, respectively, and $U_2 - U_1$ is the energy difference between state 2 and state 1.

Thus, ions will reside in the binding sites [see Fig. 2(b)] for a long time, but will pass by other sites instantaneously,[17] implying that the probability that ions reside in nonbinding sites is almost zero. This line of reasoning led to the idea of the ERINP model—that $\Psi(z)$ could be very similar to the

sum of the channel permanent potential and the ERI potentials, as shown in Fig. 1(c). To save CPU costs, the channel permanent potential was obtained by using the DELPHI [a continuum Poisson–Boltzmann (PB) solver] software package.[21] To find the positions of the resident ions, the energy minimization method was used [see Eq. (5)]. Also, the ample experimental (electron density map[5]) and theoretical (MD simulation[22,23] and BD simulation[24]) evidence that a few (two or three) K$^+$ ions always reside in the filter in the KcsA K$^+$ channel was adopted. Figure 1(c) shows how to obtain the combined potential at point (or grid point) p by adding the ERI potentials to the channel permanent potential [see Eqs. (6)–(8)]. However, as pictured in Fig. 1(d), it was very difficult to determine the potentials at the grid points inside (or around) a K$^+$ ion. For this reason, the ERI blending zone and the ERI dielectric constant (ϵ_{ERI}) were defined. The zone has a short segment with five grid points. The potentials at the two end points of the blending zone, which arise from a K$^+$ ion located at a center point of the zone, were assigned to three points inside the ion, making the potentials at all five points in the ERI blending zone the same. Therefore, the potential of the ERI blending zone was set at $ke/2$ Åϵ_{ERI} [$k = 1/4\pi\epsilon_0$, where ϵ_0 is the vacuum polarizability]. However, because an ERI blending zone of 4 Å cannot even accommodate an oxygen atom, the length of the blending zone can be extended to 6 or 8 Å to raise its reliability, in which case the formula will be set at $ke/3$ Åϵ_{ERI} or $ke/4$ Åϵ_{ERI}. To find the realistic current, the ERI dielectric constant in the blending zone is expected to be much smaller than the pore dielectric constant.[25]

C. Calculation of resident ion positions and their potentials

Because mobile ions move to minimize the free energy of the channel system, their resident positions can be determined by finding points where the total energy of the system is minimized. For instance, based on the superposition principle, the following Eq. (5) (for the two-ion state) was formulated to determine the two positions (z_i and z_j) where two K$^+$ ions most prefer to reside in the central z-axis.

$$E = \left[\phi_{z_i} + \phi_{z_j} + \frac{ke}{d_{ji}\epsilon_w} + \frac{ke}{\pi\epsilon_w} \left\{ \frac{1}{r_i} \int_0^\infty \cos\left(\frac{d_{ji}}{r_i}x\right) f(x)dx \right. \right.$$
$$\left. \left. + \frac{1}{r_j} \int_0^\infty \cos\left(\frac{d_{ji}}{r_j}x\right) f(x)dx \right\} \right] e, \tag{5}$$

where r_i and r_j are the pore radii of the channel at positions z_i and z_j, respectively, $d_{ji} = z_j - z_i$, $f(x) = (\epsilon_w - \epsilon_p)xK_0(x)$ $K_1(x)/[\epsilon_p + (\epsilon_w - \epsilon_p)xK_0(x)I_1(x)]$, ϵ_w is the dielectric constant of the channel pore, ϵ_p is the dielectric constant of the channel protein, $K_0(x)$ and $K_1(x)$ are the modified Bessel functions of the second kind, and $I_1(x)$ is the modified Bessel function of the first kind.

To find the positions with minimum energy, the cylindrical channel pore was approximated as 45 infinite cylinders of 45 varying pore radii [the length of the KcsA K$^+$ channel is 45 Å and 45 pore radii were extracted from 45 grids (1 grid in each Å)], then an analytical formula useful for calculating

the ERI induced potentials of 45 infinite cylindrical channels was adopted.[26,27] The ERI induced potential depends on the dielectric constant ratio of the channel protein to the pore protein, which is shown in $\phi_{induced}$ of Eq. (6). The formula is mathematically proven to have a solution independent of the ion radius,[28] which similarly can be applied to either a point charge or a K^+ ion that has a finite size. However, because the ERI induced potential calculated in infinite cylinders is much reduced in finite cylinders,[13] a scale factor was used to reduce the analytic potential so that the known waiting state[5,22–24] in K^+ channels is reproduced. In the two-ion state, two K^+ ions should be in the filter separated by more than 6 Å so that one water molecule is inserted between them, whereas in the three-ion state, one additional K^+ ion should be in the central cavity in a stable equilibrium. The mathematical concepts proposed for finding the combined potential at point p under the condition that two monovalent cations reside at positions i and j of the channel are utilized in Eqs. (6)–(8):

(1) If point p is not at $i-2$, $i-1$, i, $i+1$, and $i+2$ and $j-2$, $j-1$, j, $j+1$, and $j+2$, its electric potential is

$$\phi'_{z_p} = \phi_{z_p} + \frac{ke}{d_{ip}\epsilon_w} + \frac{ke}{d_{jp}\epsilon_w} + \phi_{induced}, \quad (6)$$

where $d_{ip}=z_i-z_p$, $d_{jp}=z_j-z_p$, and $\phi_{induced}=(2ke/\pi\epsilon_w) \times \{(1/r_i)\int_0^\infty \cos((d_{ip}/r_i)x)f(x)dx + (1/r_j)\int_0^\infty \cos((d_{jp}/r_j)x) \times f(x)dx\}$. Here, the first term is the channel permanent potential (obtained from DELPHI), the second and third terms are the ERI Coulomb potentials, and the fourth term is the ERI induced potential [see Fig. 4(b)], which is about an order of magnitude larger than the ERI Coulomb potential [usually less than 2 kT/e (Ref. 27)].

(2) If point p is at $i-2$, $i-1$, i, $i+1$, $i+2$, its electric potential is

$$\phi'_{z_p} = \phi_{z_p} + \frac{ke}{2 \text{ Å}\epsilon_{ERI}} + \frac{ke}{d_{jp}\epsilon_w} + \phi_{induced}, \quad (7)$$

where the second term is the electric potential of the ERI blending zone.

(3) If point p is at $j-2$, $j-1$, j, $j+1$, and $j+2$, its electric potential is

$$\phi'_{z_p} = \phi_{z_p} + \frac{ke}{2 \text{ Å}\epsilon_{ERI}} + \frac{ke}{d_{ip}\epsilon_w} + \phi_{induced} \quad (8)$$

Similarly, the modified energy formula (for the three-ion state) was formulated and applied to determine the three positions where three K^+ ions are most likely to reside.

III. DEFINING THE MODEL SYSTEM

A. Setting-up the KcsA K⁺ channel system

Figure 2(a) presents a 2D schematic of ion conductance, showing that three negatively charged major dipoles, such as the helix dipoles, the mouth dipoles, and the filter dipoles, cooperate to help the ions cross the dielectric channel. If two imaginary cubic cells are built with each side equal to 100 Å

(volume: 10^6 Å^3) in both cubic baths, there would be 84 K^+ ions and six Na^+ ions in an intracellular cubic cell, whereas there would be 84 Na^+ ions and three K^+ ions in an extracellular cubic cell. If the channel has three K^+ ions, the K^+ ion concentration of the channel becomes very high [3.51 M $=3/1440$ Å^3 (Ref. 18)], implying that the channel structure may be strongly related to its function. Figure 2(b) shows a possible waiting state for the K^+ ion conductance in K^+ channels.

B. Channel permanent potential

In this section, the method for obtaining the channel permanent potential from DELPHI is illustrated in detail. When using the grid-based PB solvers APBS and DELPHI, each point charge is divided and mapped to the surrounding grids with the dielectric constants to find the finite electric potential at every grid point. If aqueous ions are excluded, a PB solver reduces to a Poisson solver. To apply the Poisson solver to the KcsA K^+ channel, a protein data bank (PDB) file (1BL8.txt), which includes information about the KcsA protein atoms (3504 atoms or 396 amino acid residues excluding polar hydrogens[29]), was created from a PDB file of the channel (PDB accession code 1BL8). Using the Amber software package and the PDB2PQR server,[30] the PQR (protein charge and atom radius) values were determined by adding hydrogen atoms to the molecules of the channel protein to obtain the correct partial charges. To match a cubic box $(201 \times 201 \times 201$ Å$^3)$ with the geometric coordinates of the KcsA K^+ channel, the central pore line of the channel was rotated to vertical. The rotated geometric center of the channel and the center ($x=101$, $y=101$, $z=101$) of a cubic box were matched and reset to (0, 0, 0). The temperature and the ion exclusion layer around the molecule were set at 298 K and 2 Å, respectively. Then, after the dielectric constants of the channel protein and pore were set with the boundary conditions, the electric potential of each cubic box was obtained from the charge and dielectric constant information assigned to all the small cubic boxes. Note that the inside of the channel has a very strong negative electric potential enough to attract a few cations. Also, six separate potential wells were determined at an interval length of 45 Å, which ranged from point 76 to point 121 in the central z-axis [Fig. 3(b)]. The depth of the potential well progressively increased as the pore dielectric constant was reduced.

C. Combined ERI induced potential in a varying cylindrical channel

The purpose of using a varying cylindrical channel was twofold: (1) to obtain uniform conductances along the channel pore irrespective of its irregular geometry. (2) To obtain varying ERI induced potentials corresponding to the varying imaginary cylinders. In Fig. 4(b), the pore radius and the pore dielectric constant significantly affected the combined ERI induced potential arising from two K^+ ions at points 110 and 116, which ranged from 16 to 218 kT/e. When the pore dielectric constant increased, the ERI induced potential decreased, whereas, when the pore radius decreased, the ERI induced potential greatly increased.
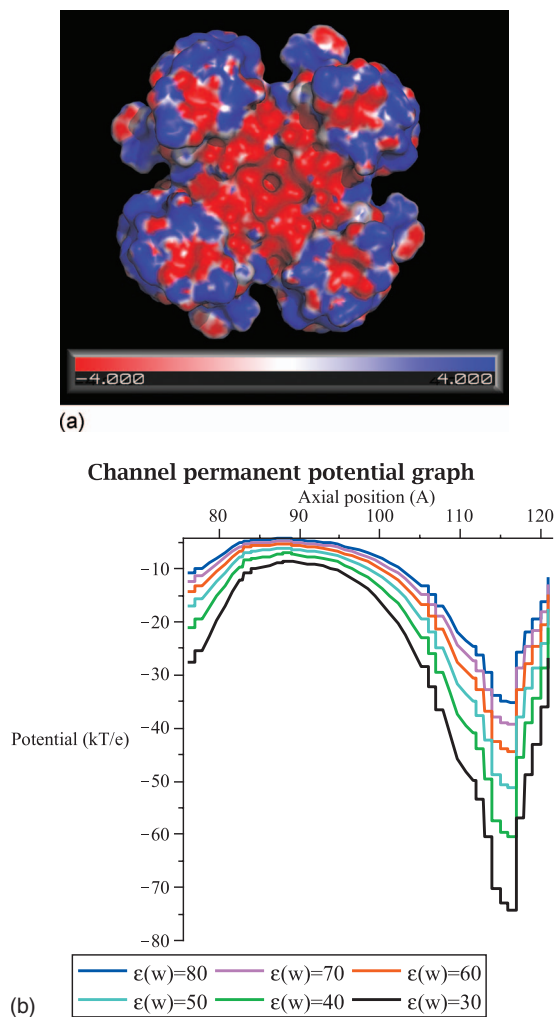
(a)

Channel permanent potential graph

(b)

FIG. 3. (a) A top view of the channel permanent potential map [determined using the APBS software package (Ref. 31)] of the KcsA K$^+$ channel (3.2 Å, PDB ID: 1BL8). Red and blue denote negative electric potential and positive electric potential, respectively. (b) The channel permanent potential graph in the central z-axis ($x=101$, $y=101,z$) of the KcsA K$^+$ channel (determined from DELPHI). The six pore dielectric constants, ranging from 30 to 80 in steps of 10, were set while maintaining a channel dielectric constant of $\epsilon_p=2$ throughout.

D. Membrane potential and K$^+$ ion concentration

Setting the concentrations of the intracellular and extracellular baths at 140 and 5 mM (using the physiological concentration in a mammalian K$^+$ channel[36]), respectively, produces a membrane potential (E) of -89.4 mV based on the Nernst equation, $E=(kT/e)\ln(|n|_{\text{out}}/|n|_{\text{in}})$. However, the resting potential of a typical animal cell is about -70–80 mV because of the small number of Na$^+$ ions that enter the channel. Setting the intracellular voltage at 100 mV and the extracellular voltage at 0 mV (an electric field of 100 mV/ 45 Å), an average drift velocity [$v=(-De/kT)(\partial\phi/\partial z)$] of 1.62 m/s was obtained, which means a K$^+$ ion requires about 2.8 ns to cross a channel with a length of 45 Å. Because the diffusion coefficient (D) inside the channel is lower than the bulk D, it is an approximate match to a physiological crossing time of 10 ns for a K$^+$ ion.[4] This indicates that both the potential and the binding time do not significantly affect the crossing time of a K$^+$ ion. The higher the concentration of K$^+$
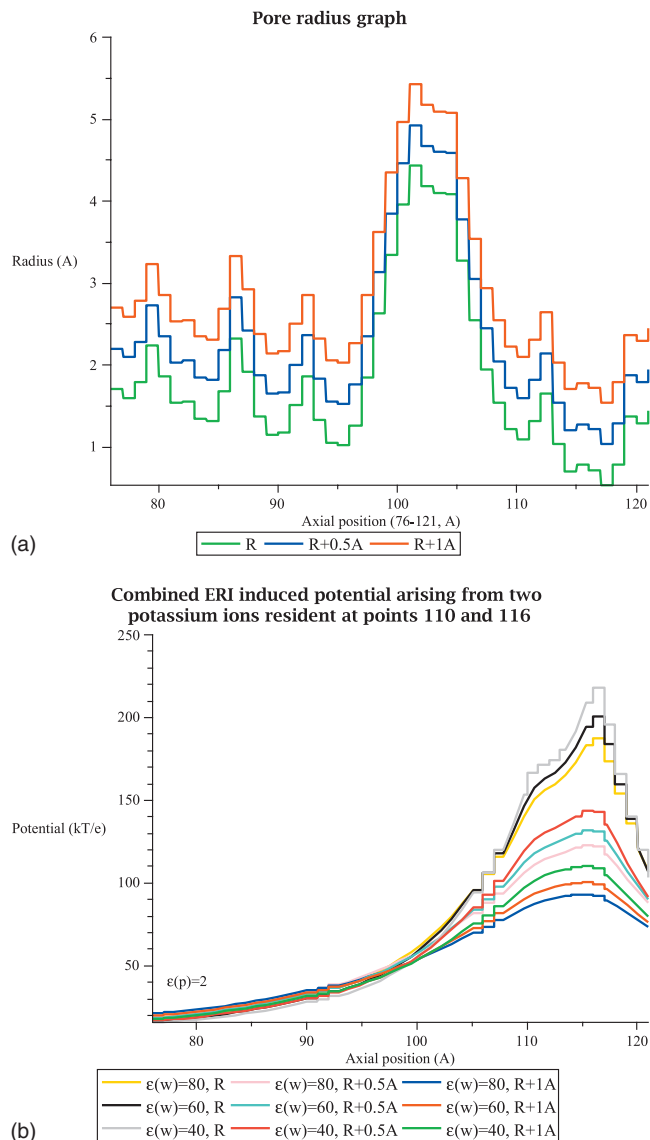
Pore radius graph

(a)

Combined ERI induced potential arising from two potassium ions resident at points 110 and 116

(b)

FIG. 4. The graph of the ERI induced potentials obtained by using three different pore radii (R, R+0.5 Å, and R+1 Å) along the central z-axis. (a) The graph of three different pore radii [determined using the Hole software package (Ref. 32)]. The pore radius was restricted to extend up to R+1 Å, which is the minimum pore radius necessary for a K$^+$ ion to cross the channel (Ref. 24). The significantly narrow pore radii of the filter indicated that the selective ion conductance of K$^+$ ions could be related to RMS fluctuations of the atoms lining the filter (Refs. 33–35). Additions of 0.5 Å and 1 Å were made to the original pore radii of the channel. (b) The combined ERI induced potential of two K$^+$ ions at points 110 and 116.

ions inside the cell, the greater chance that a K$^+$ ion will hit the channel entrance, possibly reducing the waiting time needed for a cation to reach the channel entrance. The waiting time indicates that the ion concentration does not affect the velocity of ions inside the channel [see Fig. 2(a)] because cations in an intracellular bath cannot enter the channel until a significant dielectric barrier in the channel is diminished. Therefore, the crossing time of an ion depends on the membrane potential and the channel permanent potential, whereas the waiting time depends on the membrane potential and the ion concentration on both sides of the baths. This reasoning could be explored only by considering the ion concentration a discrete entity.

TABLE I. The positions with minimum energy in both the two-ion and three-ion states (ϵ: the dielectric constant, the unit of energy: 10^{-19} J). The positions of resident ions determined when $\epsilon_w=60$ were very similar to those of the other cases, when $\epsilon_w=80$, 70, 50, 40, and 30. However, the results may be treated as reference data because the external ion concentration, the membrane potential, and the chemical environments of the channel were ignored.

State		Two-ion state		Three-ion state	
Scale factor	ϵ_w	Position	Energy	Position	Energy
1/6	60	(110, 116)	−2.68	(80, 110, 116)	−2.87
1/7	60	(110, 116)	−2.72	(80, 110, 116)	−2.93
1/8	60	(110, 116)	−2.75	(104, 100, 116)	−3.00
1/9	60	(110, 116)	−2.78	(104, 110, 116)	−3.05
1/10	60	(110, 116)	−2.79	(104, 110, 116)	−3.10

E. Technical details of channel conductance tests

The ion conductance tests on the two versus three K$^+$ ion states were performed (the tests on more than four resident ions were considered ineffectual) in the ERINP and GHK models.[5,18,22] In both models, the membrane potentials inside and outside the channel were set at 100 mV (at the left end point) and 0 mV (at the right end point), whereas the ion concentrations inside and outside the channel were set at 140 mM (at the left end point) and 5 mM (at the right end point), respectively. Note that the units of current and conductance were reported in picoampere (pA) and picosiemens (pS), respectively; 1 pA is equivalent to a flow of 6.24×10^6 K$^+$ ions/s. To plot graphs of I-V and I-C with varying voltage and ion concentrations, the applied potential was varied from −500 to 500 mV (keeping the right end point at 0 mV and changing the value at the left end point), whereas the applied concentration ranged from −1 to 1 M (keeping the right end point at 0.05 M and changing the value at the left end point). In this study, unless otherwise stated, the dielectric constants of the channel protein (ϵ_p) and pore (ϵ_w) were set at 2 and 60 (obtained from BD simulation[18,37]), respectively. Also, the diffusion coefficient (D), temperature, and radius of the channel pore were set at 1.96×10^{-9} m^2/s (for a K$^+$ ion in the bulk bath[18]), 298 K (room temperature), and R+1 Å, respectively. The computations, including plots of I-V and I-C, were performed using the mathematics software packages MATHEMATICA (Ref. 38) and MAPLE.

IV. RESULTS

A. Positions of explicit resident ions

To shed some light on how the ERI Coulomb potential, the ERI induced potential, and the ERI dielectric constant affect ion conductance, computational comparisons were performed on the two states (two-ion state and three-ion state). Because the Pauling radius of a K$^+$ ion is 1.33 Å (that of a Na$^+$ ion is 0.95 Å) and that of oxygen is 1.40 Å, they occupy three grid points in the given discretization. Thus, in a channel with a length of 45 Å, there were eight positions to test the ion-water configuration. The ion-ion configuration is excluded because two K$^+$ ions only very rarely occur with a separation distance of less than 3.5 Å.[4] Using the ERI induced potential [ϕ_{induced} of Eq. (6)] with scale factors of

1–1/10, all the possible combinations of the states were tested to determine where two and three K$^+$ ions preferred to reside. The positions of the two- and three-ion states with minimum energy (when the scale factors are 1/6-1/10) are shown in Table I. To reproduce the known waiting state in both the two-ion and three-ion states, a scale factor of 1/8 was applied to each.

B. Two versus three K$^+$ ion states

First of all, when $\epsilon_{\text{pore}}=60$, the Born energy[39] [$E_B = (e^2/8\pi\epsilon_0 R_B)(1/\epsilon_{\text{pore}}-1/80)=0.6$ kT, where R_B is 1.93 Å long for K$^+$ ions[18]] effect was ignored because it was negligible compared to a deep well energy in the channel [about −44 kT, see Fig. 3(b)]. Here, the currents (I-V: at an applied potential of 100 mV, I-C: at an applied concentration of 1 M) used for the comparisons were reduced to 1/3–1/2 of the currents displayed in the graphs of I-V and I-C because D inside the channel is about 1/3–1/2 of the bulk D (D scales linearly with the conductance).[18,20,40] For instance, when one I-V curve shows a current of 6 pA (at 100 mV), the current is reduced to 2–3 pA (by 1/3–1/2 of 6 pA) and then it is converted to a conductance of 20–30 pS (1 pS=1 pA/V).

Figure 5 is focused on the significant current changes in the I-V and I-C graphs when the ERI potentials (a scale factor of 1/8) and the ERI dielectric constant (ϵ_{ERI}) are applied. In Fig. 5(a), the effective dielectric permittivities that arise from a K$^+$ ion at three points 104 (1), 110 (2), and 116 (3) are depicted. An empirical solution[25] for the dielectric constant of water near an ion was adopted to observe the empirical change in the pore dielectric constant with distance. When $\epsilon_{\text{pore}}=80$ is assumed, the pore dielectric constants of the channel entrance remained at around 80, whereas the pore dielectric constants near a K$^+$ ion were significantly reduced. This observation confirms that the ERI dielectric constant may follow the empirical solution even when $\epsilon_{\text{pore}}=60$, which was the setting in the ion conductance tests. In Figs. 5(b)–5(f), the four colors (red, magenta, green, and blue) show the corresponding electric potentials, which would attract a third K$^+$ ion (in the two-ion state) or a fourth K$^+$ ion (in three-ion state). In Figs. 5(b) and 5(c), one blue I-V curve showed a conductance of about 37–55 pS, which matched the experimental results (conductances of about 20–250 pS[24,18,41–43]) well, whereas the GHK model curve showed a conductance of about 17–25 pS, which matched
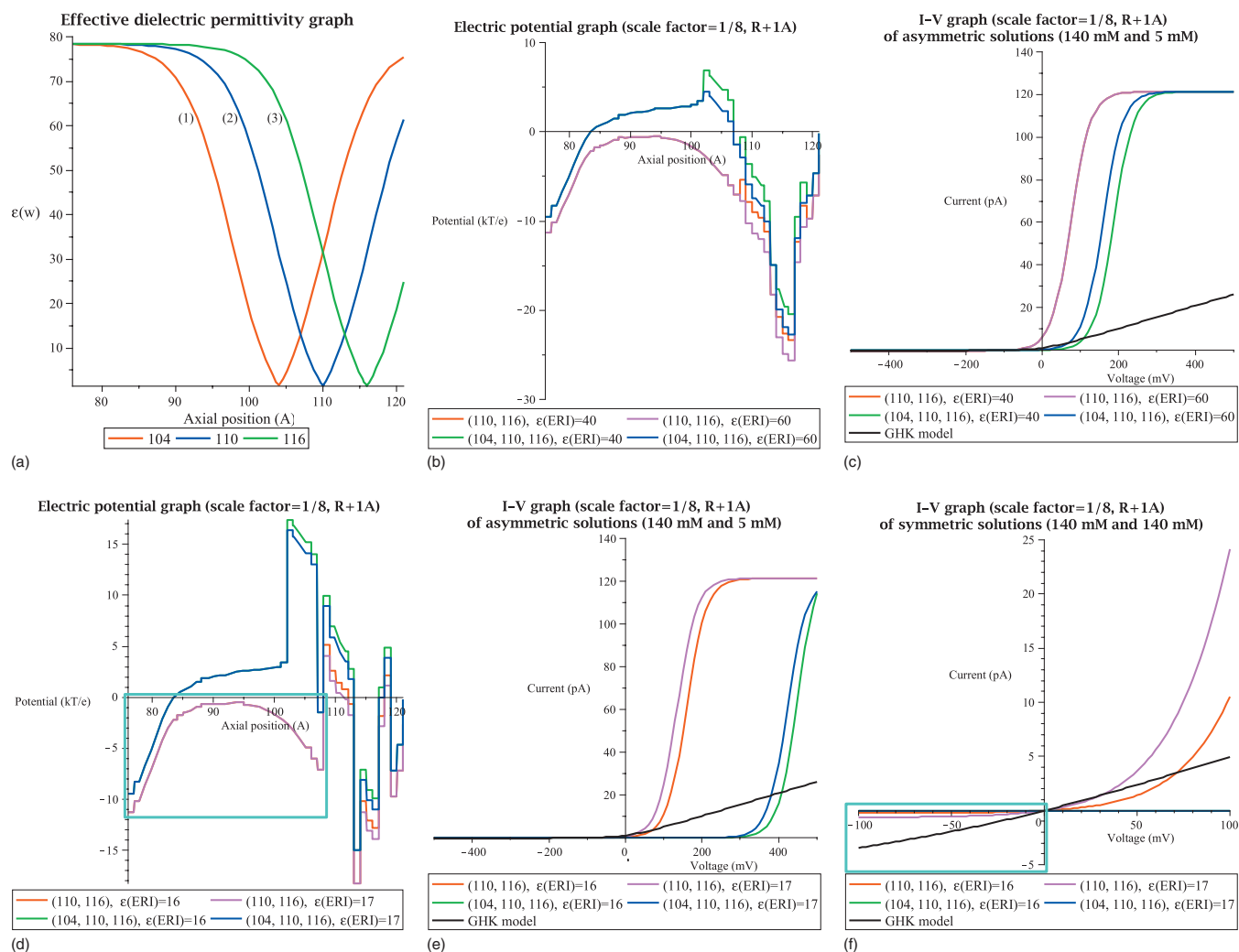
FIG. 5. (a) Effective dielectric permittivity (a function of distance from a K^+ ion) (Ref. 25). (b) The potential graph of two different states (when $\epsilon_{ERI}=40$ and 60) (c) The current-voltage (I-V) relationships of asymmetric solutions (when $\epsilon_{ERI}=40$ and 60). All I-V curves of the ERINP model are sublinear, which matched the experimental results. Both the two-ion states (red and magenta) overlapped one magenta I-V curve, which appeared to be unrealistic. (d) The potential graph of two different states (when $\epsilon_{ERI}=16$ and 17) (e) The current-voltage (I-V) relationships of asymmetric solutions (when $\epsilon_{ERI}=16$ and 17). (f) The current-voltage (I-V) relationships of symmetric solutions (when $\epsilon_{ERI}=16$ and 17). When a low ERI dielectric constant was applied, the two-ion state was much preferred over the three-ion state, which was in accord with the experimental result (Refs. 4 and 24).

the experimental results poorly. The others showed unrealistic conductances. However, the blue curve also appeared to be unrealistic because the ERI dielectric constant should be much less than 60, as depicted in Fig. 5(a). On the other hand, in Fig. 5(e), one red I-V curve showed a conductance of about 36–54 pS, whereas one magenta I-V curve showed a conductance of about 82–123 pS, resulting in an approximate match to the experimental results [a cyan box in Fig. 5(d) shows that both the two-ion states (red and magenta) still have enough negative potential to attract a third K^+ ion]. However, the I-V curves of both the three-ion states showed no conductances (at 100 mV). In Fig. 5(f), the I-V curves in symmetric solutions exhibited more reduced rectification than in asymmetric solutions (see a cyan box). However, the conductances (at 100 mV) in both the asymmetric and symmetric conditions had no significant difference. In addition, when the scale factor was decreased or the ERI dielectric constant was increased, both the I-V curves of the two- and three-ion states shifted left along the horizontal axis, and the rectification was reduced a little bit. This indicates that when

the scale factor and the ERI dielectric constant are properly applied, most experimental results can be approximately reproduced in the ERINP model.

C. Two K^+ ion state

Figure 6 shows the ion conductance (when a scale factor=1/8 and $\epsilon_{ERI}=15$, 16, and 17) in the two-ion states (110, 116) and (113, 119), which are the binding sites for the concerted ion translocation $[(1,3)\rightarrow(2,4)$ mode, see Fig. 2(b)]. Based on a knock-on mechanism,[5,44] if a third K^+ ion overcomes the barrier behind a shallow well [see the cyan box in Fig. 5(d)] and collides with the second K^+ ion, the second one pushes the first one to exit. Thus, if the ERI potentials exceed the binding potential barriers, the new two-ion state replaces the previous one.[5] In Figs. 6(a) and 6(b), the state (110, 116) of the conditional Poisson (CP) model, which was simulated using DELPHI under the condition that two K^+ ions resided in the filter, produced no current in both the I-V and I-C graphs because of two spurious

I–V graph (scale factor=1/8) of asymmetric solutions (140 mM and 5 mM)

—— CP (113, 119),	—— ERINP (110, 116), ϵ(ERI)=16, R+1A
—— ERINP (110, 116), ϵ(ERI)=15, R+1A	—— ERINP (110, 116), ϵ(ERI)=17, R+1A
—— ERINP (113, 119), ϵ(ERI)=16, R+1A	—— ERINP (110, 116), ϵ(ERI)=16, R+0.5A
—— ERINP (110, 116), ϵ(ERI)=16, R	—— GHK model, R+1A

(a)

I–C graph (scale factor=1/8) of asymmetric potentials (100 mV and 0 mV)

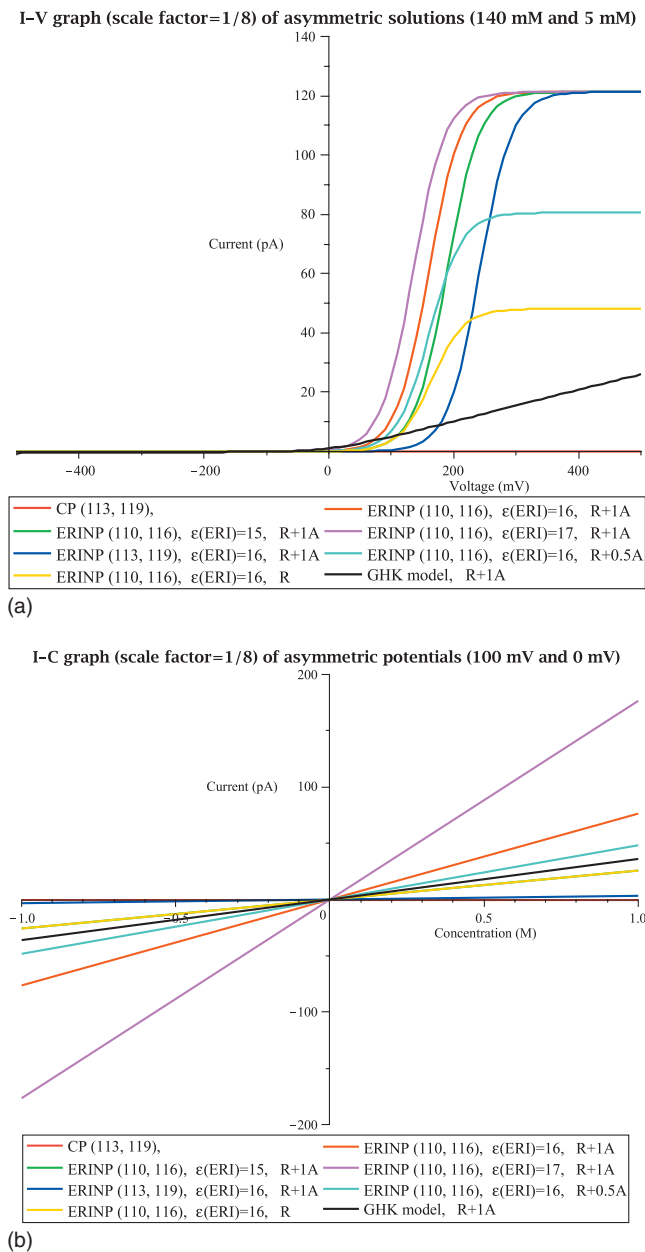|	
—— CP (113, 119),	—— ERINP (110, 116), ϵ(ERI)=16, R+1A
—— ERINP (110, 116), ϵ(ERI)=15, R+1A	—— ERINP (110, 116), ϵ(ERI)=17, R+1A
—— ERINP (113, 119), ϵ(ERI)=16, R+1A	—— ERINP (110, 116), ϵ(ERI)=16, R+0.5A
—— ERINP (110, 116), ϵ(ERI)=16, R	—— GHK model, R+1A

(b)

FIG. 6. (a) The current-voltage (*I-V*) relationships of asymmetric solutions (when $\epsilon_{ERI}=15$, 16, and 17) in the ERINP model, the GHK model, and the CP model. (b) The current-concentration (*I-C*) relationships of asymmetric solutions (when $\epsilon_{ERI}=15$, 16, and 17) in the ERINP model, the GHK model, and the CP model. Note that the real shape of *I-C* curves (or lines) is sublinear, so saturated, obeying the Michaelis–Menten function (Refs. [1] and [29]), $I=I_{max}/1+[K_s]/[K]$ where $[K_s]$ denotes the half-saturation point of the ion channel and $[K]$ is the concentration of the K$^+$ ions. Both the two-ion states denoted in yellow and green overlapped one yellow *I-C* curve, showing unrealistic conductances.

self-potentials[12] at points 110 and 116, pointing out a weakness of the continuum application of explicit resident ions. In addition, when $\epsilon_{ERI}=16$ and the pore R+1 Å, state (110, 116) produced more conductance than state (113, 119), indicating that state (110, 116) with minimum energy is related to high ionic throughput. When $\epsilon_{ERI}=16$, the conductances of state (110, 116) obtained by using three different pore radii (R, R+0.5 Å, and R+1 Å) were proportional to the corresponding pore radii. Like the red and magenta *I-V* curves, which matched the experimental results fairly well

[reported in Fig. 5(e)], one cyan *I-V* curve was an approximate match to the experimental results, showing conductances of about 23–34 pS (at 100 mV) and about 110–165 pS (at 200 mV). In addition, one yellow *I-V* curve showed a conductance of about 64–96 pS (at 200 mV), which was also an approximate match to the experimental results. The others showed more or less unrealistic conductances. In Fig. 6(b), the red and cyan *I-C* curves showed conductances of about 256–384 pS and about 161–241 pS (at 1 M), respectively, which approximately matched the experimental results [conductances of 200–300 pS (Ref. [43])], whereas the others showed more or less unrealistic conductances. However, there is no state seeming to exhibit a realistically saturated conductance, indicating that the ERINP model, like the other continuum models, also fails to describe the saturated current-concentration relationships. Note that the ion state and the ion conductance appeared to be very sensitive to small changes in the ERI potentials, the ERI dielectric constant, the ERI locations, and the pore radius. In summary, although the GHK model also provides some useful information, the ERINP model has the following advantages over the GHK model: (1) it matches most experimental results using flexible parameters; (2) it provides an in-depth look into the channel system using the discrete entities of ions such as the ERI potentials and the ERI dielectric constant; and (3) it provides biologically significant information that the traditional continuum model cannot, which is summarized in Sec V.

D. Nonlinear dynamics of a K$^+$ ion crossing the KcsA K$^+$ channel

The result stating that the ERINP model produces more current than the GHK model gives rise to the question: What is the intrinsic role of the channel permanent potential? To address this question, a mathematical analysis of the K$^+$ ion dynamics was performed. Assume that a single K$^+$ ion of mass m crosses along the central z-axis of a cylindrical vacuum channel under an electric field of 100 mV/45 Å. As the K$^+$ ion approaches the channel entrance with an initial velocity of 1.62 m/s (about 0 Å/ps), it is attracted by a shallow well (potential energy of about -14 kT) in the channel entrance because the influential area of a deep well (potential energy of about -44 kT) is limited only inside the channel. Figure 7 illustrates the nonlinear dynamics of K$^+$ ions crossing the channel. In Fig. 7(a), the graph of electric potential obtained from DELPHI (when $\epsilon_p=2$ and $\epsilon_w=60$) was plotted. Once a K$^+$ ion enters the channel, the ion (a filled green circle) will proceed toward the bottom of a deep well that holds two K$^+$ ions in a stable configuration by climbing over a shallow well.[18] Also, when the ion enters the filter, its velocity is at its maximum because of a deep well, following the approximate conservation of energy $[E=(1/2)my[z(t)]^2+V[z(t)]$; t denotes time, y denotes the velocity, and V denotes the electric potential energy]. Thus, a deep well not only compensates for the ERI induced potentials that arise because of traversing K$^+$ ions, but it also speeds up K$^+$ ions so that they enter the filter with maximum kinetic energy. In Fig. 7(b), the numerical electric force $[V'(z)]$ graph shows
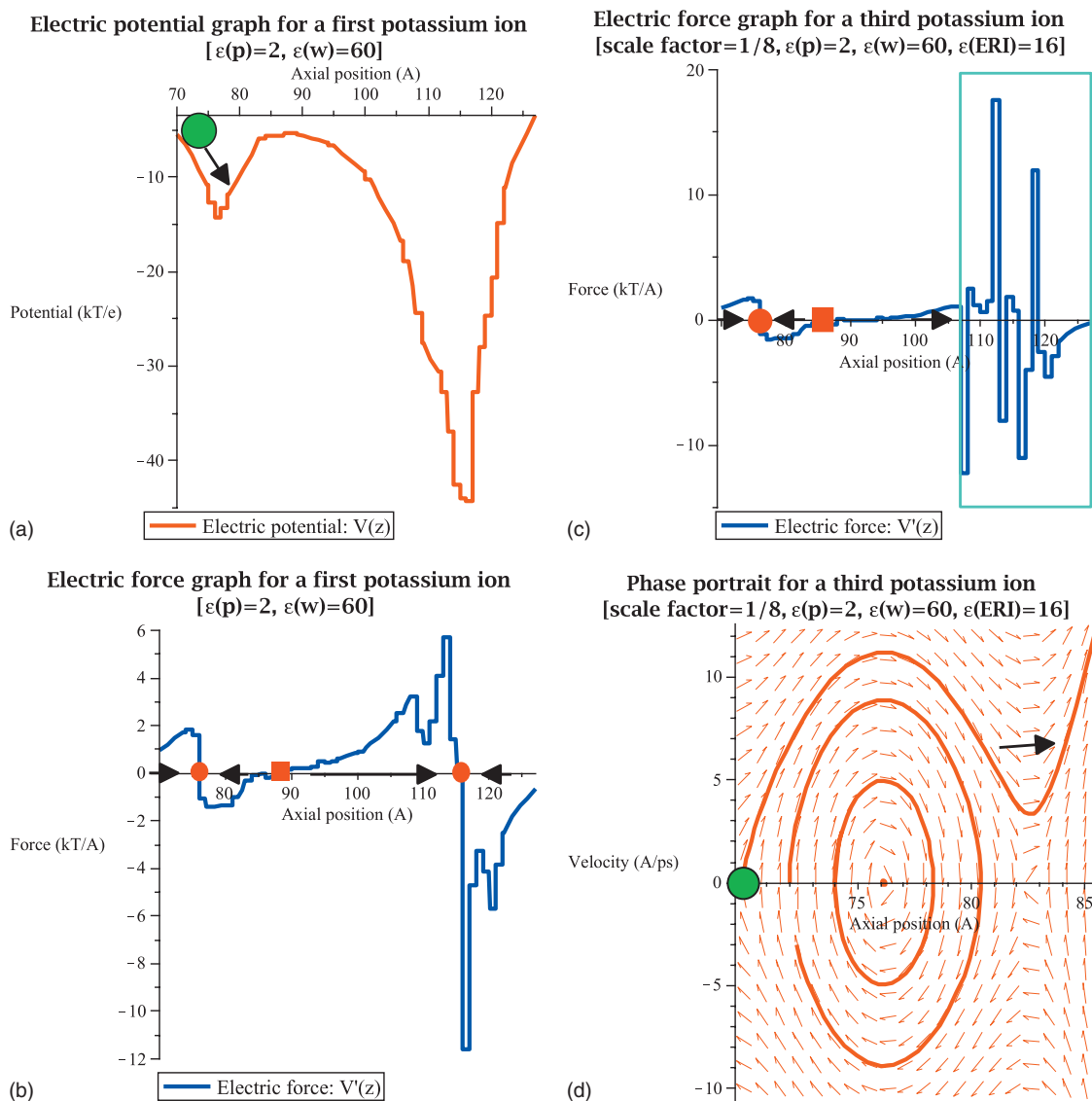
FIG. 7. (a) A K$^+$ ion in a double-well potential of the central z-axis (when there is no ion resident inside the channel). (b) Electric force of the central z-axis (when there is no ion resident inside the channel). (c) Electric force of the central z-axis (when there are two K$^+$ ion resident at points 100 and 116 inside the channel). (d) The phase portrait of a K$^+$ ion climbing over a shallow well produced by the ring of mouth dipoles (Ref. 18) (in three picoseconds). Because there exists no deep well because of the ERI potentials, the ion can cross the channel.

that two stable nonlinear center points (filled red circles) are found at points 76 and 116, whereas an unstable saddle point (a filled red rectangle) is found at point 88. The graph also shows that the channel has a strategic structure (or charge distribution) that favors outward rectification of conductances, with a long length in the forward direction and a short length in the backward direction. Here, the black arrows denote the direction of a moving ion, and the positive force helps the ion move forward, whereas the negative force helps the ion move backward. In Fig. 7(c), the $V'(z)$ graph obtained from the condition in which two K$^+$ ions reside at points 110 and 116 shows that the positive and negative electric forces in the cyan box appear to be canceled out. In Fig. 7(d), a phase portrait using the discrete $V'(z)$ graph in Fig. 7(c) was depicted. The phase portrait, which is based on the conservation of energy, describes possible K$^+$ ion trajectories in mathematical terms. To create a continuous function for the discrete $V'(z)$, the electric forces of four discrete points

within a shallow well, which ranged from point 70 to point 85 in the central z-axis, were selected and connected by using the Lagrange interpolation polynomials. Then a numerically approximated phase portrait was plotted using the vector field of $dz/dt=y$ and $dy/dt=-V'(z)/m$. Given the condition that the positive and negative electric forces in the cyan box shown in Fig. 7(c) are approximately canceled out, the phase portrait provides a possible pattern for how a third K$^+$ ion climbs out of a shallow well and moves across the remaining part of the pore rapidly[24] to achieve the ion conductance that is balanced by the channel permanent potential and the ERI potentials.

V. CONCLUSIONS AND DISCUSSION

The current obtained from the 1D model was expected to be similar to that in the 3D model because the channel permanent potential used in the ERINP model was extracted

from the DELPHI 3D data. Current is thought of as an accumulation of ion flow[45] affected by the specific chemical and electrostatic interactions between atoms in the physical system including the protein atoms, water, and ions. Thus, there is no mechanism to perfectly integrate these phenomena into a model. Most significantly, when calculating the ERI induced potential, some errors must arise in approximating the cylindrical channel pore using 45 infinite cylinders of 45 varying pore radii. However, the approximations of the scaled ERI induced potential would be enough to elucidate the conductance mechanism without losing crucial information. Also, though the ERI dielectric constant was applied, assigning a uniform pore dielectric constant to the entire pore except the ERI blending zone was only an approximation; in fact, a large approximation was made for the filter. The main conclusions of the study can be summarized as follows:

(1) The ERINP model was formulated to reproduce a more realistic electric field inside the channel using the ERI potentials and the ERI dielectric constant in a cylindrical channel of varying $A(z)$.

(2) The ERINP model can explicitly take into account the effects of resident ions inside the KcsA K^+ channel, and maintain the advantage in computational efficiency of the continuum modeling approach.

(3) The ion state and the ion conductance appeared to be greatly influenced by the ERI potentials and the ERI dielectric constant, as well as by the ERI locations and the pore radius. In particular, when the ERI dielectric constant was applied, the two-ion state was much preferred over the three-ion state, which was in accord with the experimental result.

(4) Despite the simplifying assumptions of the ERINP model, the model significantly improved data reliability in the NP-type conductance model and reproduced most experimental results with a realistic set of parameters including the ERI potentials and the ERI dielectric constant.

(5) A mathematical analysis of the K^+ ion dynamics illustrated a tight structure-function system with a shallow well, a deep well, and two K^+ ions resident in the filter.

ACKNOWLEDGMENTS

[1] B. Hille, *Ion Channels of Excitable Membranes* (Sinauer, Sunderland, MA, 2001).

[2] L. Anson, Nature (London) **440**, 439 (2006).

[3] D. P. Chen, V. Barcilon, and R. S. Eisenberg, Biophys. J. **61**, 1372 (1992).

[4] J. H. Morais-Cabral, Y. Zhou, and R. MacKinnon, Nature (London) **414**, 37 (2001).

[5] D. A. Doyle, J. M. Cabral, R. A. Pfuetzner, J. M. G. A. Kuo, S. L. Cohen, B. T. Chait, and R. MacKinnon, Science **280**, 69 (1998).

[6] B. Corry, S. Kuyucak, and S. H. Chung, J. Gen. Physiol. **114**, 597 (1999).

[7] S. Edwards, B. Corry, S. Kuyucak, and S. H. Chung, Biophys. J. **83**, 1348 (2002).

[8] P. Graf, M. G. Kurnikova, R. D. Coalson, and A. Nitzan, J. Phys. Chem. B **108**, 2006 (2004).

[9] U. Hollerbach, B. Nadler, Z. Schuss, and R. S. Eisenberg, Phys. Rev. E **70**, 051912 (2004).

[10] S. H. Chung and B. Corry, Soft Matter **1**, 417 (2005).

[11] B. Z. Lu, Y. C. Zhou, G. A. Huber, S. D. Bond, M. J. Holst, and J. A. McCammon, J. Chem. Phys. **127**, 135102 (2007).

[12] B. Corry, S. Kuyucak, and S. H. Chung, Biophys. J. **84**, 3594 (2003).

[13] S. Kuyucak, O. S. Andersen, and S. H. Chung, Rep. Prog. Phys. **64**, 1427 (2001).

[14] OPENDX, http://www.opendx.org.

[15] D. E. Goldman, J. Gen. Physiol. **27**, 37 (1943).

[16] B. Roux, Biophys. J. **77**, 139 (1999).

[17] S. C. Li, M. Hoyles, S. Kuyucak, and S. H. Chung, Biophys. J. **74**, 37 (1998).

[18] S. H. Chung, T. W. Allen, M. Hoyles, and S. Kuyucak, Biophys. J. **77**, 2517 (1999).

[19] B. Corry, S. Kuyucak, and S. H. Chung, Biophys. J. **78**, 2364 (2000).

[20] S. Furini, F. Zerbetto, and S. Cavalcanti, Biophys. J. **91**, 3162 (2006).

[21] W. Rocchia, E. Alexov, and B. Honig, J. Phys. Chem. B **105**, 6507 (2001).

[22] C. E. Capener and M. S. Sansom, J. Phys. Chem. B **106**, 4543 (2002).

[23] S. Bernèche and B. Roux, Biophys. J. **78**, 2900 (2000).

[24] S. H. Chung, T. W. Allen, and S. Kuyucak, Biophys. J. **82**, 628 (2002).

[25] E. L. Mehler and E. Eichele, Biochemistry **23**, 3887 (1984).

[26] T. Bastug and S. Kuyucak, Biophys. J. **84**, 2871 (2003).

[27] R. Wijesinghe, N. Coorey, and S. Kuyucaka, J. Chem. Phys. **127**, 195102 (2007).

[28] B. Nadler, U. Hollerbach, and R. S. Eisenberg, Phys. Rev. E **68**, 021905 (2003).

[29] V. Krishnamurthy and S. H. Chung, Proc. IEEE **95**, 853 (2007).

[30] T. J. Dolinsky, J. E. Nielsen, J. A. McCammon, and N. A. Baker, Nucleic Acids Res. **32**, W665 (2004).

[31] N. A. Baker, D. Sept, S. Joseph, M. J. Holst, and J. A. McCammon, Proc. Natl. Acad. Sci. U.S.A. **98**, 10037 (2001).

[32] O. S. Smart, J. M. Goodfellow, and B. A. Wallace, Biophys. J. **65**, 2455 (1993).

[33] B. Roux, Annu. Rev. Biophys. Biomol. Struct. **34**, 153 (2005).

[34] S. Y. Noskov and B. Roux, Biophys. Chem. **124**, 279 (2006).

[35] T. W. Allen, O. Andersen, and B. Roux, J. Gen. Physiol. **124**, 679 (2004).

[36] D. Johnston and S. M.-S. Wu, *Foundations of Cellular Neurophysiology* (MIT Press, Cambridge, MA, 1994).

[37] J. A. Ng, T. Vora, V. Krishnamurthy, and S. H. Chung, Eur. Biophys. J. **37**, 213 (2008).

[38] S. Wolfram, *Mathematica*, 2nd ed. (Addison-Wesley, Reading, 1991).

[39] M. Born, Z. Phys. **1**, 45 (1920).

[40] S. H. Chung and S. Kuyucak, Biochim. Biophys. Acta **1565**, 267 (2002).

[41] J. Farley and B. Rudy, Biophys. J. **53**, 919 (1988).

[42] H. Schrempf, O. Schmidt, R. Kummerlin, S. Hinnah, D. Muller, M. Betzler, T. Steinkamp, and R. Wagner, EMBO J. **14**, 5170 (1995).

[43] M. LeMasurier, L. Heginbotham, and C. Miller, J. Gen. Physiol. **118**, 303 (2001).

[44] A. L. Hodgkin and R. D. Keynes, J. Physiol. (London) **128**, 61 (1955).

[45] R. Elber, D. P. Chen, D. Rojewsk, and R. Eisenberg, Biophys. J. **68**, 906 (1995).